Bubble dynamics near the onset of single-bubble sonoluminescence

Charles R. Thomas,* Ronald A. Roy, and R. Glynn Holt
Department of Aerospace and Mechanical Engineering, Boston University, Boston, Massachusetts 02215, USA
(Received 16 June 2004; published 1 December 2004)

A number of groups have reported measurements of the location in the parameter space of bubble size versus acoustic pressure amplitude of shape- and size-stable bubbles. For air/water systems, a general trend emerges: stable bubbles are found on one of two line paths in this space defined by their range of acoustic pressure. Bubbles on the higher-pressure path emit light. There have been few studies of the transition between these two paths. In this work we describe our observations of this transition regime. In this regime, a slow time scale oscillation (period 2–7 s) in the bubble size, position, and phase of flash timing can be observed. At lower dissolved gas concentrations, a hysteresis in the bubble size as a function of acoustic pressure is observed, complementing previous light intensity measurements reported in the literature.

DOI: 10.1103/PhysRevE.70.066301 PACS number(s): 47.55.Dz, 43.25.+y, 78.60.Mq

I. INTRODUCTION

Light emission from a single, acoustically driven bubble [single-bubble sonoluminescence (SBSL)] was first achieved in the early 1990s [1]. This achievement was one of many efforts made by researchers [2–9] to simplify the study of multiple-bubble sonoluminescence (MBSL), which was discovered in the early 1930s [10]. Compared to the random nature of the light emission in MBSL the light emission from a SBSL bubble was found to be remarkably steady, and thus easier to study. Since 1990 a number of different groups [11–14] have made measurements in the parameter space of equilibrium size (either R_0 or $R_{\max}$) and acoustic pressure amplitude (P_a) to locate the position of stable bubbles. These groups have worked at a variety of different external control parameters [e.g., driving frequency, ambient pressure, temperature, and dissolved gas concentration (DGC)]. Although the absolute numbers differ, the general picture that has emerged is shown in Fig. 1. Stable bubbles fall along two lines in the parameter space. Following [11] we will refer to these lines as the lower branch and the upper branch. All of the bubbles on these lines are size and shape stable; however, only bubbles on the upper branch emit measurable light. To date, there has been little investigation of the transition between the lower and upper branches, which marks the onset of SBSL. Therefore, in the present work, we report measurements of the maximum radius as a function of acoustic pressure in this transition regime.

II. APPARATUS

A schematic of the equipment used in the experiment is shown in Fig. 2. The camera and lens are focused on the bubble, which levitates at the center of the cell. The light-emitting diode (LED) (wavelength ≈590 nm) provides light for backlighting the bubble for video imaging. Imaging is accomplished using a long distance microscope (Infinity, K2) and charge-coupled device (CCD) camera (Sony, XC-75). An optical filter (Oriel, No. 51664) mounted in front of the photomultiplier tube (PMT) (Phillips, XP2262B) blocks the transmission of light from the LED to the PMT; this arrangement allows for simultaneous light emission measurement and video imaging. The transducer (PZT) (EDO Ceramics, EC-64) is cooled with a small computer fan. The hydrophone (3 in. Uncopiers needle hydrophone) monitors the acoustic pressure in the cell. The dark square beneath the cell and PZT represents a three-axis motorized positioning system (Kollmorgen-NEAT, *z* stage, ZE-100-SM; *x*-*y* stage, XYR-6060). During experimental runs, the cell, PMT, and lens-camera system are placed in a light-tight enclosure, indicated by the dashed line in Fig. 2.

The oscilloscope allows for real-time monitoring of fast-time scale signals (acoustic pressure and light emission pulses). A filter (Krohn-Hite, 3940) is used to amplify and to eliminate high frequency noise from the hydrophone signal.

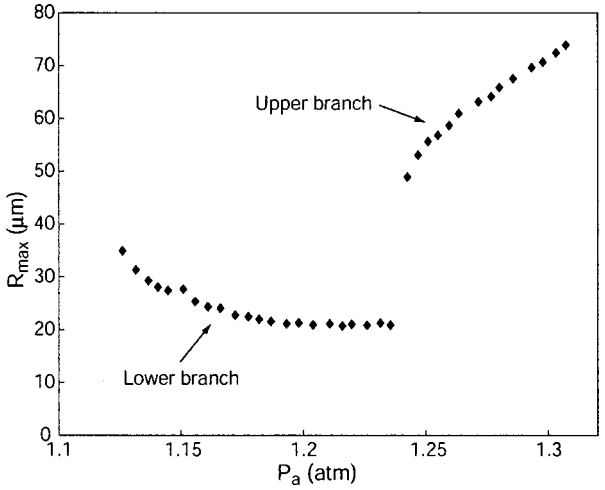

FIG. 1. Plot showing the location of stable bubbles in $P_a, R_{\max}$ parameter space for DGC approximately 0.0015 and driving frequency 14.620 kHz.

*Electronic address: crt@bu.edu

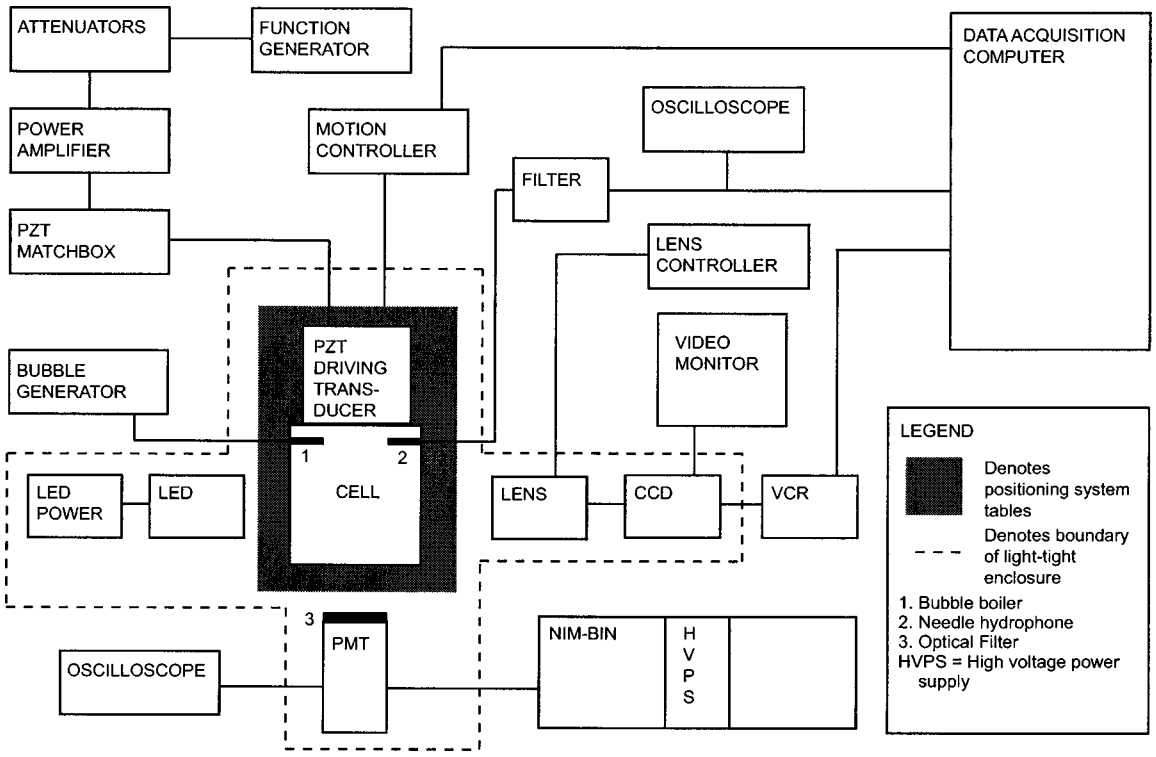

FIG. 2. Schematic showing equipment used in the experiment. The dashed line indicates the boundary of a light-tight enclosure.

The lens used in the experiment was equipped with motorized control of zoom and focus. The power amplifier (ENI, 1040L) amplifies the driving voltage from the function generator (HP, 33120A); this amplified signal is input to the PZ driving transducer through an impedance matchbox (ENI, EVB-1).

Attenuators (JFW, 50R-019) are used to vary the signal range generated by the function generator. The NIM-BIN (Tennelec, TB3) serves as a power supply for the high voltage power supply (Bertan, 362) which provides a large bias voltage to the PMT. Images from the CCD camera are recorded on the VCR (Sony, SVO-2100) during experimental runs for post-data-collection analysis. The video monitor (Dot-X) displays the field of view of the camera. The bubble generator power supply (custom built) provides power to a boiling bubble generator, which is mounted in the cell.

The data-acquisition computer (Computers for Everyone, Cambridge, MA), using the data-acquisition software LABVIEW (National Instruments), orchestrated time-tagged data acquisition via two analog-to-digital (A/D) boards (National Instruments, NI6023E and NI6070), two serial ports and a general purpose interface bus board (GPIB) (National Instruments, PCI-GPIB).

The cell used in the experiments was cube shaped, approximately 3 in. on each side. For all of the experiments described here, the cell was run at 14.620 kHz. At this frequency the $(n_x, n_y, n_z) = (1, 1, 1)$ mode of the cell was excited, so there was a pressure maximum in the center of the cell; the bubble levitated slightly above this location.

III. EXPERIMENTAL PROCEDURES

The cell was filled with degassed water (the estimated DGC was[1] 0.0015). Then, using this water the location of stable bubbles in the $(P_a, R_{\max})$ space was measured in the following manner. First a bubble was established in the growth and breakup regime [1], and then the acoustic pressure was increased by increasing the PZT voltage in steps until the extinction threshold was reached. After reaching the extinction threshold, the acoustic pressure was reduced slightly and a new bubble was created. The pressure was then decreased in steps until the growth and breakup regime was returned to. For each pressure step, 30 images of the bubble were acquired by a frame grabber (Epix, PIXCI-SV4, not shown in the schematic) for postexperiment analysis. During the entire experimental run the VCR recorded images of the bubble (as a backup for the images acquired directly by the frame grabber). After the conclusion of data acquisition, the water was left in the cell, and the experiment was repeated at five later times (spaced by 6–12 h), for a total of six data acquisition runs. During these waiting periods, gas dissolved into the water through a 4 mm diameter hole (it was through this hole that the hydrophone was inserted into the cell). As a result the DGC of the water increased; thus the parameter space for a range of DGC's was measured. The amount of time ($\approx$1 h) that it took to perform an entire ex-

[1]The method by which the DGC was estimated is described in detail in [25].

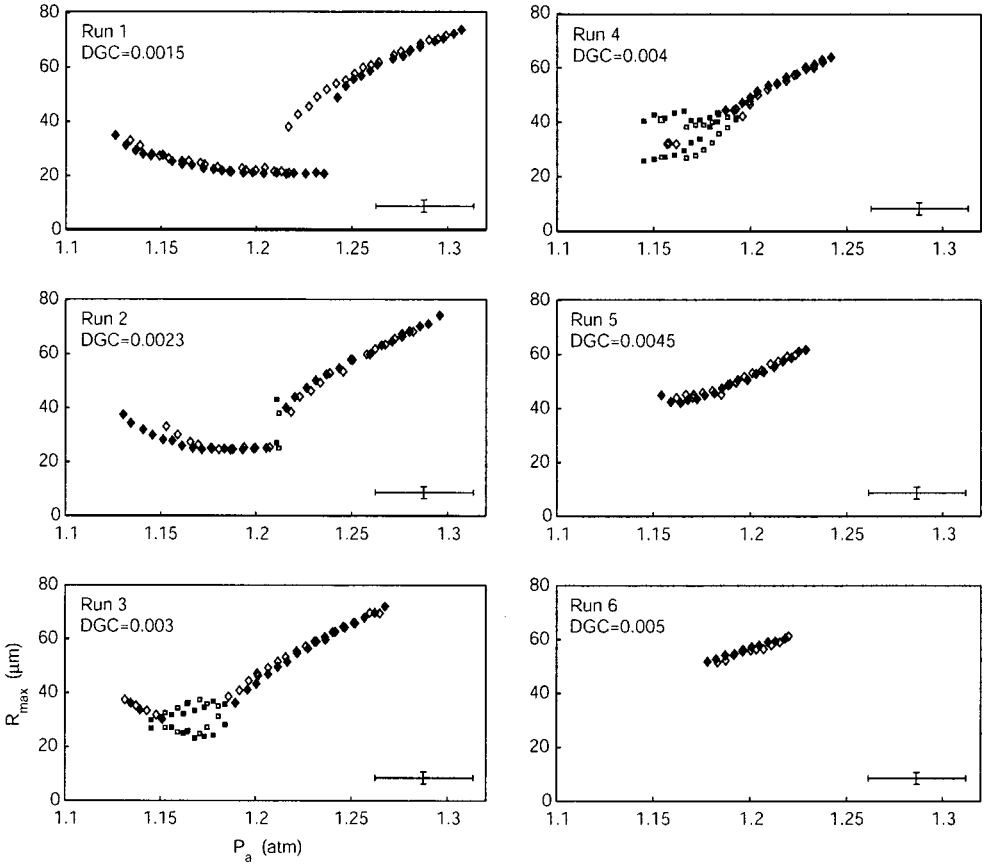

FIG. 3. Plots showing the location of shape-stable bubbles, both light-emitting and non-light-emitting. Filled symbols indicate data taken while the acoustic pressure was increased and open symbols indicate data taken when the acoustic pressure was decreased. The estimated DGC for each run is noted on the plot. Diamonds indicate size stable equilibrium positions and squares indicate the end points of the equilibrium oscillations described in the text. The acoustic pressure error bar represents the total uncertainty in the acoustic pressure, given by the calibration process; the acoustic pressure resolution is much smaller, approximately ±0.005 atm. The R_{max} error bar is the resolution uncertainty of R_{max}.

perimental run was small enough to consider the DGC to be constant during the run.

Typically, for each acoustic pressure visited while taking data the bubble would attain a steady-state (nonchanging) equilibrium radius after a short transient (the length of the transient depends on the acoustic pressure and the DGC). There were, however, some acoustic pressures and DGCs for which the bubble did not reach a steady-state size. Instead the bubble grew and shrank periodically while being driven at a *constant* acoustic pressure. As it changed in size, its position also changed. These transitions from growing to shrinking and back to growing are smooth; furthermore, the bubble does not break up via shape instabilities.

The oscillation states occurred at the transition from the lower branch to the upper branch for a range of DGCs. To study the oscillations more closely, after the mapping experiments were completed the cell was refilled with water which had the correct DGC in order to observe the oscillations. For these experiments, in addition to all the measurements mentioned above, the phase of the light emission and acoustic emission relative to the sound cycle were measured.

The video images (for the nonoscillating pressures) were processed using the image analysis software X-CAP (Epix), and the data were saved to text files. The images of the bubble in the oscillating state required a different processing technique. X-CAP was used to control the VCR so that a frame-by-frame analysis could be done, and thus the time-dependent maximum radius and position of the bubble could be measured.

IV. RESULTS AND DISCUSSION

A. Parameter space maps

Figure 3 shows the results of the mapping experiments. Since no active temperature control was used,[2] the temperature of the water was not constant; however, from run to run the largest difference was only 2 °C, and in any single run the temperature changed by a maximum of only 0.7 °C. The

[2]A passive type of temperature control was implemented, however—during the experiments, the air conditioning in the laboratory was set to its minimum control point which resulted in an air temperature of anywhere between roughly 16 and 18 °C.

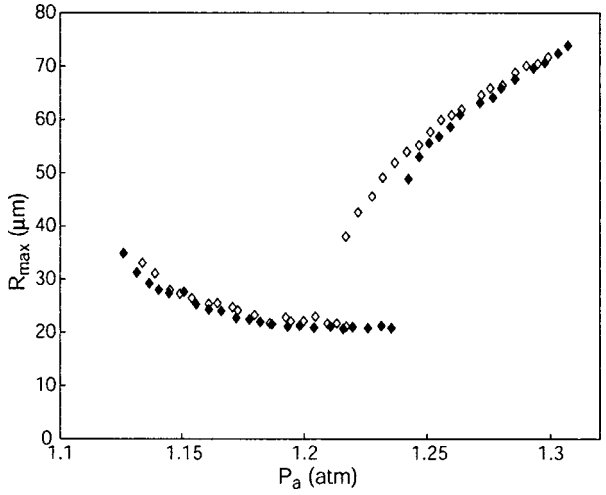

FIG. 4. Plot showing the location of shape- and mass-stable bubbles from mapping run 1. Filled symbols indicate data taken while the acoustic pressure was increased and open symbols indicate data taken while the acoustic pressure was decreased.

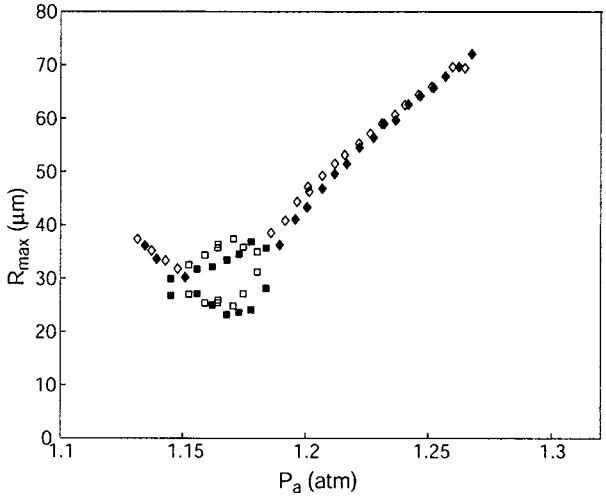

FIG. 5. Plot showing the location of shape-stable bubbles from mapping run 3. The filled symbols indicate data taken while the acoustic pressure was increased. The open symbols indicate data taken while the acoustic pressure was decreased. The diamonds indicate a mass-stable bubble (one that does not change in equilibrium size at a constant pressure) and the squares indicate the extrema of the oscillations described in the text.

ambient pressure varied by less than 0.08 atm from run to run.[3]

For ease of discussion, the plot of the first data run (DGC$\approx$0.0015) is shown again in Fig. 4. The lower branch (left side of the plot) is where stability arises from the balance of chemical reactions and diffusion according to the dissociation hypothesis [15,16]. No detectable light is emitted on the lower branch. The upper branch is where stable SL occurs, on the right side of the plot.

Looking at the plot, perhaps the most interesting feature is that for a small range of acoustic pressures (roughly 1.22 to 1.24 atm) the data for increasing acoustic pressure do not follow the same path as that for decreasing acoustic pressure, i.e., there is a hysteresis in the maximum bubble radius at these pressures. A hysteresis in the light emission has been observed previously by Asai and Watanabe [17] and they attributed it to a hysteresis in the equilibrium bubble size; however, no measurements of the bubble size were made during those experiments. During the present experiments the light emission was measured as well. These measurements also exhibited hysteresis which was very similar to that reported by Asai and Watanabe. The hysteresis was predicted by the dissociation hypothesis (see specifically [18]), and its existence can be understood by considering the content of a bubble on either side of the hysteresis. On the right side of the hysteresis (the upper branch) the bubble contains mainly argon. The collapse of the wall is energetic enough to dissociate all species other than noble gasses, and can provide energy to promote the emission of light. On the left side of the hysteresis (the lower branch) the bubble contains air. At the acoustic pressure amplitudes on the lower branch the collapse of the bubble wall is not energetic enough to dissociate non-noble gas species and promote light emission.

[3]The temperature of the water was measured with a thermocouple mounted in the cell. The ambient pressure was measured by a pressure transducer mounted near the cell.

In addition to the hysteresis observed in run 1, another interesting feature in the bubble behavior was a slow (compared to the acoustic period) oscillation in the equilibrium size of the bubble observed in runs 2, 3, and 4. Figure 5 shows the map from run 3 (DGC$\approx$0.003). Recall that the major difference between this run and run 1 is the DGC: the DGC of the water for run 3 is higher than the DGC for run 1. Notice that the hysteresis has disappeared (this dependence on gas concentration was also noticed by Asai and Watanabe). There is, however, a new feature in Fig. 5: the squares in the pressure range $\approx$1.15 to 1.19 atm. At these pressures a time-periodic oscillation in the equilibrium bubble size accompanied by a periodic translation oscillation was observed. The upper squares denote the maximum R_{max} value of this oscillation and the lower squares denote the minimum R_{max} of the oscillation. These size oscillations had a typical period of 2–7 s. The observation of a spontaneous size oscillation somewhat similar to the current oscillation was briefly reported in [19,20]. It should be noted that the extent of the oscillation regime grows (notice that only two pressures in data run 2 exhibit oscillations) and then disappears as a function of increasing DGC.

Another observation, which has been reported previously (see [11]), is that the lower branch disappears as a function of increasing DGC. The disappearance can be understood by consideration of the chemistry that is happening in the bubble. Compared to water with a small DGC, more gas per cycle can diffuse into a bubble in water with a higher DGC. Thus the acoustic pressure at which the increase in size caused by diffusion is balanced by the losses due to the chemical reactions must increase. It so happens that, for example in run 5, the smallest acoustic pressure for which chemistry balances diffusion is the same acoustic pressure that is required for the bubble to be on the upper branch.

Finally, notice that the maximum acoustic pressure for which a stable light-emitting bubble can exist gets smaller as

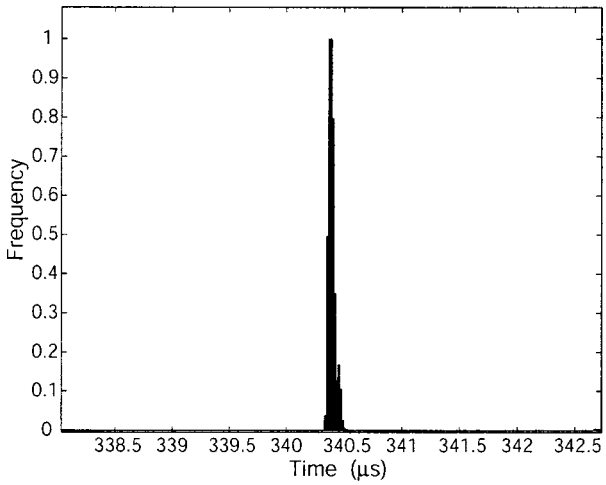

FIG. 6. Histogram of light emission times for a stable SL bubble. While the data for this histogram were taken, the acoustic pressure was 1.30 ± 0.05 atm and the DGC was estimated to be about 0.003. The sample size of the histogram is 26 247 samples with a peak value of 6372, at 340.3880 ms. The histogram is plotted normalized by the peak value. The time is relative to the trigger of the oscilloscope. The measurements system did not record every pulse of light from the bubble during this run. The total time for the run was around 5 min.

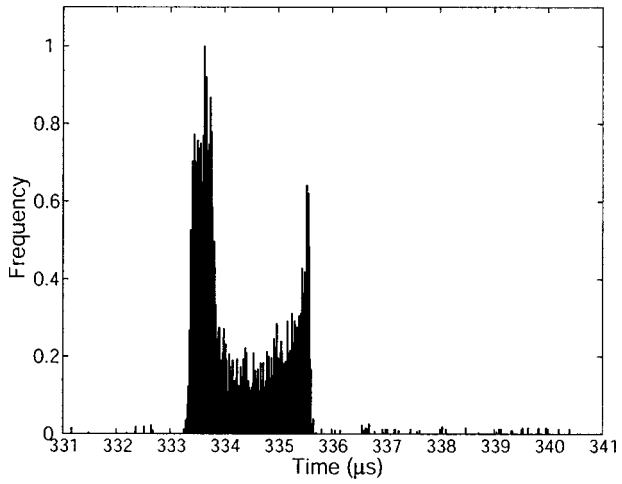

FIG. 7. Histogram of light emission times for an oscillating SL bubble. $P_a = 1.15 \pm 0.05$ atm, and the estimated DGC was about 0.003. The sample size for this histogram was 12 780 samples, with a maximum of 305 at time 333.6285 ms. As in Fig. 6, data have been normalized to the maximum count. The total time for data collection was about 20 min.

a function of increasing DGC. The reduction is due to the fact that the shape instability threshold [11,21,22] intersects the upper branch at lower pressures for higher DGCs.

The slow equilibrium oscillations were an unexpected discovery, and therefore they were studied in more detail; the results of these measurements are the subject of the next section.

B. Pulse timing and equilibrium oscillations

Two bubbles of different equilibrium radii driven at the same acoustic pressure will collapse at different times, and thus the phase of light emission with respect to the acoustic pressure phase for each bubble will be different; with this in mind it was expected that if measurements of the phase of light emission were made for bubbles in the oscillating regime and a histogram were computed using this data, the histogram would not have a single well defined maximum as in the case for stable SBSL (see Fig. 6). The data shown in this section were acquired during a different experimental run (but with similar DGC values) than the data presented in the previous section; however, the same behavior as depicted in Fig. 3 was observed. Figure 6 is a plot of the histogram of flash times for a stable bubble driven at an acoustic pressure of 1.30 ± 0.05 atm and DGC of about 0.003. The full width at half maximum (FWHM) of the distribution in Fig. 6 is about 40 ns. The width is a function of the jitter of the phase of the bubble and the electronics (both the sound generation electronics and the measurement electronics) used to instrument the experiment. Since other groups [23,24] have measured much smaller times for the distribution of the phase of collapse of a stable SBSL bubble, the FWHM quoted above should be interpreted as mainly characterizing the resolution of the experimental apparatus and not the phase distribution of the light emission of the bubble.

After collecting the data that comprise the histogram in Fig. 6 the acoustic pressure was decreased until an oscillating state was observed. The acoustic pressure was decreased (instead of increased) because the oscillation region is at the transition from the lower to upper branch. The pulse time histogram for such a state is shown in Fig. 7. The histogram looks remarkably similar to Fig. 2(d) in [23]—a broad distribution with two peaks on either side. In [23] Holt *et al.* postulated that the broad distribution might be the result of the bubble changing its equilibrium size. They did not measure the bubble size; however, the bubble size along with the position and the arrival time of the acoustic emission from the collapsing bubble[4] were measured simultaneously in the current experiment. Time series of these four quantities (taken from data acquired while the histogram in Fig. 7 was acquired) are shown in Fig. 8. Clearly, the broad histogram is the result of a periodic oscillation of the equilibrium bubble size. The range of the histogram is roughly 2.3 μs, which is nearly the same as the peak-to-peak amplitude of the acoustic pulse arrival time (denoted τ_a). The maximum bubble radius varies with the same frequency (in this case about 0.5 Hz) as τ_a, as do the bubble's z and x direction positions in the field of view. When the acoustic pressure was increased slightly the bubble moved to a stable state on the upper branch.

Figure 9 shows a plot of the vertical position of the bubble vs the horizontal position of the bubble for the time series shown in Fig. 8. It was noticed that during the oscillations the bubble remained in focus—since the focal depth of the lens was small compared to the extent of the y and z direction motions, the motion was either an ellipse with a

[4]The method by which the arrival time of the acoustic pulse was measured is described in excruciating detail in [25].

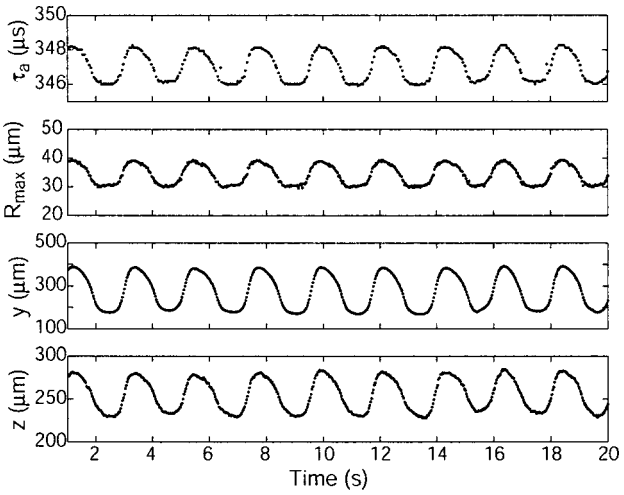

FIG. 8. Plots of the oscillation in (a) the arrival time of the acoustic pulse (τ_a), (b) $R_{\max}$, (c) the horizontal position, and (d) the vertical position, for the bubble which produced the histogram shown in Fig. 7.

very small minor axis (compared to its major axis) or a line.

Some other interesting features of the oscillation of the four quantities mentioned above are shown below in Figs. 10–12. The data for these particular time series were taken during a different experimental run than Fig. 8 so the external parameters might appear to be inconsistent (i.e., the acoustic pressure for one of the series is the same as for the case discussed above, but the behavior is different). This apparent inconsistency is because of the difficulty of performing repeatable measurements with the current system, especially when the water is changed. Although the precision uncertainty in acoustic pressure amplitude within a run is clearly ±0.005 atm or better, by calculating the total uncertainty in the acoustic pressure measurement in the fashion that has been adopted (considering accuracy not just precision; see [25]) we account for this lack of run-to-run repeatability. For each of these four data runs, the ambient pressure

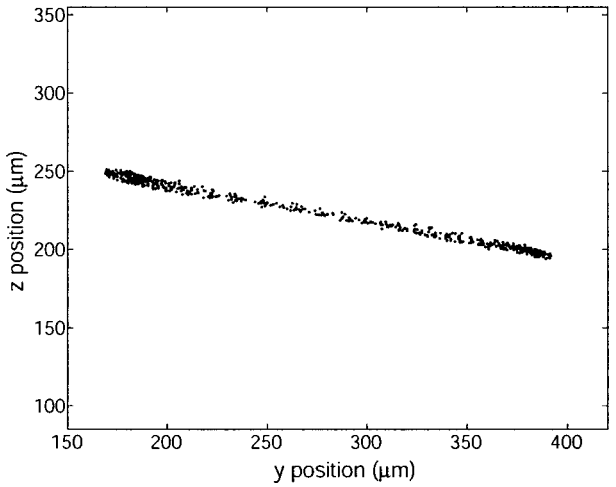

FIG. 9. Plot of z position (vertical on screen) vs y position (horizontal on screen) of bubble in an oscillatory state (data taken from the same set as for Fig. 8).

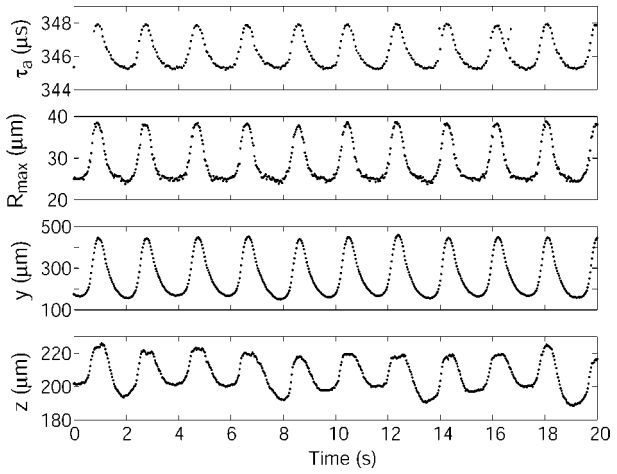

FIG. 10. Plots of oscillations when $P_a = 1.15 \pm 0.05$ atm.

was measured to be 0.99 atm, and the temperature was 26 °C. The acoustic pressure for the data plotted in Fig. 10 was 1.15 ± 0.05 atm, and the DGC was again near 0.003. There was some light emission from the bubble; however, for the amount of time that data were collected it did not produce a statistically significant histogram. The frequency of oscillation was again about 0.5 Hz; however, there are some differences between these data and the data plotted in Fig. 8. The most obvious difference is that the troughs of the oscillations are wider than the peaks: the bubble spent more time at a smaller radius than at a larger radius. Notice also that although τ_a is periodic it appears that the position of the bubble over time (seen most clearly in the z component) has a lower frequency response equal to about $1/3$ of the fundamental τ_a frequency. This subharmonic lasted only for the length of time displayed here (the data run continued for about 25 s longer). In the next time series presented in Fig. 11, the acoustic pressure was lower than in the previous two (1.11 ± 0.05 atm). The oscillations begin in a fairly linear fashion (the amount of time the bubble spends at the troughs is roughly equal to the time at the crests) but at about 25 s, a subharmonic appears in the dynamics. There was a very small amount of light emission—even less than in Fig. 10,

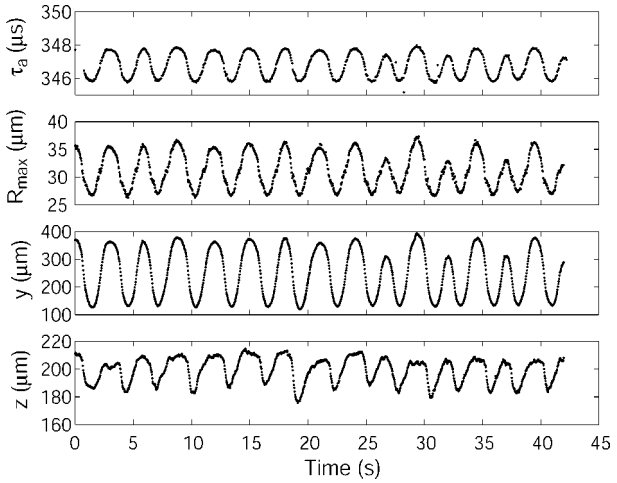

FIG. 11. Plots of oscillation when $P_a = 1.11 \pm 0.05$ atm.

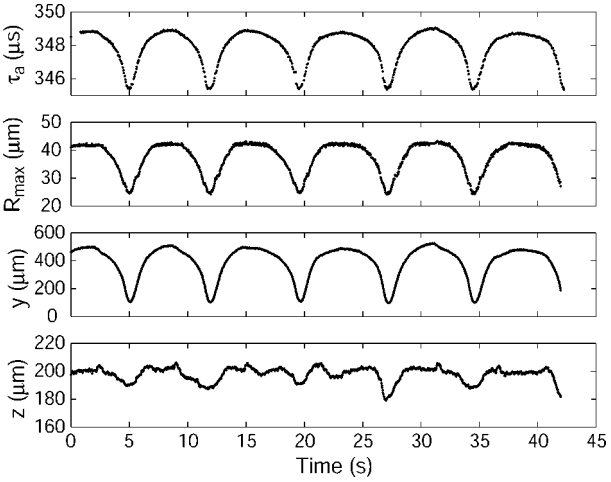

FIG. 12. Oscillation for $P_a = 1.09 \pm 0.05$ atm.

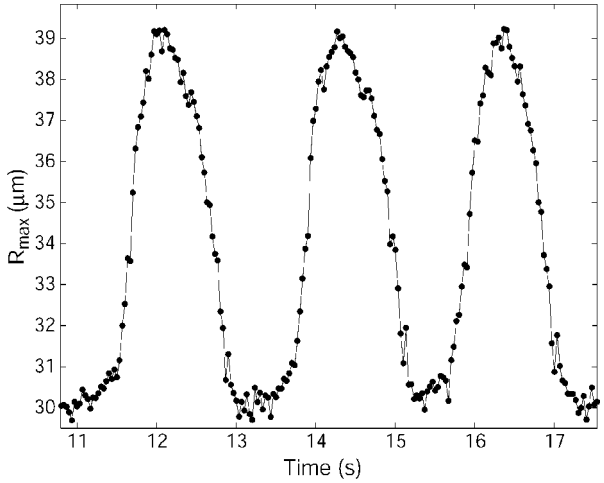

FIG. 13. Plot showing the oscillation in $R_{\max}$ for three cycles. The data were taken from those plotted in Fig. 8. The lines connecting the points are a guide for the eye.

which is not surprising because the acoustic pressure is smaller and so the temperatures achieved during collapse are smaller. The frequency of the fundamental of the oscillation at this pressure was about 0.3 Hz, which mirrors the general trend: the frequency of oscillation decreases with decreasing acoustic pressure.

At an even lower acoustic pressure (1.09 ± 0.05 atm), the behavior of the oscillation changed drastically (Fig. 12). The frequency of oscillation in this case was about 0.14 Hz. It was clear in this data run that when the bubble attained its maximum radius, it was very close to breaking up; however, just when it was expected to hit the shape instability threshold (this known from experience), it began to shrink in size and thus was stabilized. Soon after the data collection for this acoustic pressure ended, the oscillation ended and the bubble did begin a growth and breakup cycle from which it did not emerge.

It should be noted here that although the oscillations were repeatable, i.e., they appeared always at roughly the same pressure amplitude (the transition from the lower branch to the upper branch) and range of DGCs, the absolute behavior of the oscillations was not; this can be seen by comparing the peak-to-peak amplitude of the time series data to the data in the maps.

We summarize the general findings.

(1) The oscillation frequency was observed to decrease with decreasing acoustic pressure.

(2) The oscillations at acoustic pressures close to the minimum that permitted a stable bubble on the upper branch were more robust than oscillations at lower acoustic pressures.

(3) The changing size of the bubble influences the collapse time and this causes the light to be emitted at a range of times.

(4) Oscillations appear only in a range of DGC defined by the onset (for decreasing DGC) of hysteresis.

It might be argued that the oscillation in size is a result of the bubble translation: when the bubble moves to a different position, the local acoustic pressure changes, and thus the bubble should adjust its equilibrium radius according to the Eller-Flynn [26] rectified diffusion theory. However, the measured change in acoustic pressure of the fundamental frequency is very small—too small to effect such a large change in bubble size. Consider the data in Fig. 12; the amplitude of the oscillation in $R_{\max}$ is roughly 20 μm and the maximum change in position of the bubble [equal to $D_{osc}^{\max}\sqrt{(y_{pp}^2+z_{pp}^2}$, where the subscript *pp* denotes peak-to-peak amplitude] is about 400 μm. The pressure profile in the *z* direction in the cell was measured to vary as $P_a^{\max}\cos(k_z z_a)$, with $k_z = \pi/L_z = \pi/0.087\,142\ \mathrm{m} = 36.011\ \mathrm{m}^{-1}$. Since the cell is cubic the variation in the *y* and *x* directions is taken to be the same. Since the bubble is within the vicinity of the pressure maximum, an estimate for the change in acoustic pressure because of the change in position is $\cos(k_z D_{ocs}^{\max})$. Substituting values, this is equal to 0.9999; thus if the pressure at the position of the bubble when it is at its smallest radius is 1.15 atm, it will be 1.149 885 at the position of the bubble when it is at its largest radius. Thus the *change* in the acoustic pressure is only 1.15×10^{-4} atm. Examining the maps (Fig. 3) it can be seen that to effect a 20 μm change in the maximum radius a much larger acoustic pressure change is needed (≈ 0.04 atm). Considering the foregoing analysis, it is not unreasonable to conclude that these oscillations are taking place at a constant acoustic pressure amplitude. We did not observe evidence of higher frequency components of the acoustic field as observed by [27].

Recall that the dissociation hypothesis predicts that when on the lower branch, the mass loss because of chemical reactions can balance the mass gain from diffusion each cycle. Furthermore, on the upper branch the temperatures are such that the chemical reactions can overcome the diffusion. It is postulated that the oscillations are the result of a more complex interplay between diffusion and chemistry, so instead of balancing each other or one dominating the other over an acoustic cycle, their relative influences change on a slow time scale. Three cycles of the oscillation in $R_{\max}$ taken from Fig. 8 are plotted in Fig. 13.

At $t = 12$ s, the bubble is at its maximum radius; at this time the growth from diffusion has slowed down and the

effects due to chemical reaction are beginning to become dominant. Chemical effects become dominant perhaps because there are now enough species to react and thus the reactions can take place, i.e., the reactions are not starved. When the bubble reaches its minimum R_{max} the maximum temperatures generated by the bubble collapse are not as high, and the bubble can grow because of diffusion. At this time, the cycle begins anew. The bubble translates because of its change in size: since the time-averaged volume of the bubble changes the buoyant force must change as well. To remain levitated the bubble must move to a different position where the Bjerknes force can balance the buoyant force. Again, this is not the whole story since the bubble translates roughly five times more in the lateral direction than the vertical direction in Fig. 12. Although it is not attempted in this work, we contend that a model including time-dependent chemistry and diffusive effects, coupled with the body forces on the bubble, might be able to explain these oscillations. Such a model has already shown promise in explaining other features of SBSL systems.

V. CONCLUSION

The experiments described in the current work were performed using water with a range of DGCs. The lowest DGC revealed the existence of a hysteresis in the bubble size as a function of increasing and decreasing acoustic pressure. The existence of the hysteresis is explained [18] by the different thermodynamic conditions in and chemical makeup of the bubble on either side of the threshold for light emission. The hysteresis was also observed in the light emission of the bubble, which has been reported previously [17]. As in Ref. [17] the hysteresis was found to disappear when the DGC increased; however, in the current work, with its disappearance another interesting phenomenon appeared: a time-dependent oscillation of the equilibrium radius at constant acoustic pressure.

It is hypothesized that the oscillations are a result of the competing effects of chemical reactions in the bubble and diffusion of gas from the host water. Measurements of the flash timing from a bubble in an oscillatory state revealed that these bubble-size oscillations had been observed before [23], albeit indirectly. Instead of emitting light at the same time every acoustic cycle (as in stable SL) bubbles in an oscillatory state emit light at a range of times: the histogram of pulse times from an oscillating bubble will not have a single peak, but instead a broad distribution. The frequency of the oscillation (on the order of 500 mHz) is incommensurable to the driving frequency; therefore the resulting light emission exhibits a quasiperiodic oscillation. These observations provide an explanation for two of the three dynamic behaviors observed in [23]: quasiperiodicity and (most probably) chaos in the light emission. The SL, occurring once per cycle, illuminated the effects of a reaction-diffusion system in a regime that is diffusion controlled. The period doubling in the flash timing in [23] remains an unsolved mystery [28].

It is important to note that the oscillations can exist only if the dissolved gas in the water is air (or some mixture that mimics air): there can be no chemical reactions if there are no species to react. As such, the oscillations cannot be observed in systems other than air/water systems. We suggest the reason the observation of these oscillations has not been reported previously is that most researchers have been more interested in studying the brightest possible bubbles—which occur in water at acoustic pressure amplitudes higher than the ones near the onset of SBSL; thus these interesting oscillations are often overlooked.

ACKNOWLEDGMENT

The authors gratefully acknowledge the financial support of NASA.

[1] D. F. Gaitan, Ph.D. dissertation, The University of Mississippi, Oxford, 1990.
[2] J. Schmid, Acustica **9**, 321 (1959) (in German).
[3] J. Schmid, Acustica **12**, 70 (1962) (in German).
[4] C. Wang and Z. D. Zhang, Acta Acust. (Beijing) **1**, 59 (1964) (in Chinese).
[5] F. B. Peterson and T. P. Anderson, Phys. Fluids **10**, 874 (1967).
[6] T. Saksena and W. Nyborg, J. Chem. Phys. **53**, 1722 (1970).
[7] P. R. Temple, M.S. thesis, University of Vermont, 1970.
[8] C. D. Ohl, O. Lindau, and W. Lauterborn, Phys. Rev. Lett. **80**, 393 (1998).
[9] T. Leighton, W. Ho, and R. Flaxman, Ultrasonics **35**, 339 (1997).
[10] N. Marinesco and J. Trillat, C. R. Hebd. Seances Acad. Sci. **196**, 858 (1933) (in French).
[11] R. G. Holt and D. F. Gaitan, Phys. Rev. Lett. **77**, 3791 (1996).
[12] B. Barber, R. Hiller, R. Löfstedt, S. Putterman, and K. Weninger, Phys. Rep. **281**, 66 (1997).
[13] J. Ketterling and R. Apfel, Phys. Rev. E **61**, 3832 (2000).
[14] G. Simon, I. Csabai, A. Harváth, and F. Szalai, Phys. Rev. E **63**, 026301 (2003).
[15] D. Lohse, M. Brenner, T. Dupont, S. Hilgenfeldt, and B. Johnston, Phys. Rev. Lett. **78**, 1359 (1997).
[16] D. Lohse and S. Hilgenfeldt, J. Chem. Phys. **107**, 6986 (1997).
[17] T. Asai and Y. Watanabe, Jpn. J. Appl. Phys., Part 1 **39**, 2969 (2000).
[18] R. Toegel and D. Lohse, J. Chem. Phys. **118**, 1863 (2003).
[19] R. G. Holt and D. F. Gaitan, J. Acoust. Soc. Am. **101**, 3060 (1997).
[20] R. G. Holt and D. F. Gaitan, Bull. Am. Phys. Soc. **41**(9), 1693 (1996).
[21] Y. Hao and A. Prosperetti, Phys. Fluids **11**, 1309 (1999).
[22] S. Hilgenfeldt, D. Lohse, and M. Brenner, Phys. Fluids **8**, 2808 (1999).
[23] R. G. Holt, D. F. Gaitan, A. Atchley, and J. Holzfuss, Phys.

Rev. Lett. **72**, 1376 (1994).
[24] B. P. Barber, Ph.D. dissertation, University of California, Los Angeles, 1992.
[25] C. R. Thomas, Ph.D. dissertation, Boston University, Boston, 2004.
[26] A. Eller and H. G. Flynn, J. Acoust. Soc. Am. **37**, 493 (1965).
[27] J. Holzfuss, M. Rüggeberg, and R. G. Holt, Phys. Rev. E **66**, 046630 (2002).
[28] M. Levinsen, N. Weppenaar, J. Dam, G. Simon, and M. Skogstad, Phys. Rev. E **68**, 035303(R) (2003).